Research Square

Preprints are preliminary reports that have not undergone peer review.
They should not be considered conclusive, used to inform clinical practice,
or referenced by the media as validated information.

Recapitulating SARS-CoV-2 Infection in a Human Lung Organoid-on-a-Chip at the Air-Liquid Interface

Sohyun Park
Seoul National University Bundang Hospital
So-Hui Kim
Pusan National University
Bokyong Kim
Seoul National University Bundang Hospital
Eun-Young Eo
Seoul National University Bundang Hospital
Hyung-Jun Kim
Seoul National University Bundang Hospital
Yuhui Jeong
Pusan National University
Jeongbin Park
jeongbin.park@pusan.ac.kr

Pusan National University
Young-Jae Cho
Seoul National University Bundang Hospital

Research Article

Keywords: Lung organoid-on-a-chip, Air-liquid interface, SARS-CoV-2, Lung organoids, Lung-on-a-chip, Single-cell RNA sequencing

Posted Date: August 20th, 2026

DOI: https://doi.org/10.21203/rs.3.rs-10547160/v1

License: This work is licensed under a Creative Commons Attribution 4.0 International License.
Read Full License

Additional Declarations: No competing interests reported.

Recapitulating SARS-CoV-2 Infection in a Human Lung Organoid-on-a-Chip at the Air-Liquid Interface

Sohyun Park[1,2,†], So-Hui Kim[3,†], Bokyong Kim[1], Eun-Young Eo[1], Hyung-Jun Kim[1], Yuhui Jeong[4], Jeongbin Park[3,4*], Young-Jae Cho[1,2,*]

†These authors contributed equally to this work as co-first authors.

**These authors jointly supervised this work as co-corresponding authors.*

[1]Division of Pulmonary and Critical Care Medicine, Department of Internal Medicine, Seoul National University College of Medicine, Seoul National University Bundang Hospital, Seongnam-si, Gyeonggi-do, Republic of Korea

[2]Department of Health Science and Technology, Graduate School of Convergence Science and Technology, Seoul National University, Gwanak-gu, Seoul, Republic of Korea

[3]Interdisciplinary Program of Genomic Data Science, Pusan National University, Yangsan-si, Gyeongsangnam-do, Republic of Korea

[4]School of Biomedical Convergence Engineering, Pusan National University, Yangsan-si, Gyeongsangnam-do, Republic of Korea

***Correspondence:**

Jeongbin Park

jeongbin.park@pusan.ac.kr

Young-Jae Cho

lungdrcho@snu.ac.kr

Keywords: Lung organoid-on-a-chip; Air-liquid interface; SARS-CoV-2; Lung organoids; Lung-on-a-chip; Single-cell RNA sequencing

Abstract

Background: Chronic respiratory diseases and emerging pathogens such as SARS-CoV-2 are a major global health burden. Traditional in vitro models, however, poorly recapitulate the functional complexity of the human lung, limiting mechanistic study and therapeutic development.

Methods: To address this, we developed a lung organoid-on-a-chip in which patient-derived airway organoids are differentiated at an air–liquid interface and co-cultured with vascular endothelial cells and macrophages on a microfluidic platform. The chip was infected with four SARS-CoV-2 variants - Wuhan, Delta, Omicron BA.1, and Omicron XBB.1 - and profiled by single-cell RNA sequencing.

Results: The platform reconstituted native airway cellular composition within an air–liquid interface, and single-cell profiling revealed pronounced epithelial remodeling, including loss of ciliated cells, blunted interferon responses, and partial epithelial-to-mesenchymal transition priming. This was accompanied by an endothelial angiogenic response marked by an expanded angiogenic tip-like state and a VEGF-independent angiogenic-ligand program, with these responses remaining consistent across all four variants.

Conclusions: Collectively, this lung organoid-on-a-chip recapitulates conserved SARS-CoV-2 epithelial and vascular responses, providing a physiologically relevant platform for respiratory disease research.

Background

The global burden of respiratory diseases continues to rise, even excluding the impact of COVID-19. Chronic respiratory diseases, such as chronic obstructive pulmonary disease (COPD), asthma, pneumoconiosis, interstitial lung disease (ILD), and pulmonary sarcoidosis, remain significant causes of morbidity and mortality, with risk factors like smoking, air pollutants, and occupational hazards. In addition to this, COVID-19 can act as an independent predictor of severity and higher mortality in patients with COPD and ILD, while also causing long-term fibrotic-like changes in the lungs. In 2019, an estimated 4 million deaths were attributed to chronic respiratory conditions, with 454.6 million people affected worldwide [1,2,3]. In lung disease research, in vitro 2D cell cultures and animal models have been widely used, but they lack the ability in replicating the intricate architecture, function of human tissues, and microenvironment cues. These shortcomings highlight the importance of developing advanced 3D models, such as lung organoids and lung-on-a-chip systems, which better mimic the biophysical and biochemical characteristics of human lung tissue [4,5]. Among these advanced models, organoids are particularly valuable as they closely replicate *in vivo* cell-to-cell interactions and extracellular matrix (ECM) communication. 3D organoid models, derived from stem cells, can self-organize into multi-cellular structures that closely mimic vivo environment and allow for the proliferation and differentiation of stem cells into structures resembling the corresponding adult tissue [6,7]. Although 3D organoids offer valuable insights into lung disease, they still face challenges, particularly in the complete differentiation of lung cell types and mimicking the mechanical forces experienced during breathing. To address these gaps, Air-Liquid Interface (ALI) models were developed to improve ciliated cell differentiation and enhance epithelial function, making them crucial for studying diseases where epithelial functionality is vital [8]. Lung organoid-on-a-chip technology further advances this by

integrating microfluidics with 3D lung models to replicate both the structural and dynamic aspects of lung physiology, such as airflow and mechanical stretching, creating a more accurate tool for disease modeling and drug testing [9]. The combination of Lung organoid-on-a-chip and ALI systems more closely simulates the lung environment, enhancing mucociliary differentiation and epithelial barrier function, while also allowing for efficient testing platform that offers an ethically viable alternative to animal models. In the context of infectious diseases, particularly given the global impact of SARS-CoV-2, the development of robust in vitro models has become increasingly crucial. The Lung organoid-on-a-chip not only enables the replication of SARS-CoV-2 infection under controlled conditions but also allows for real-time imaging and tracking of viral dynamics. This technology serves as a highly valuable tool for investigating virus-host cell interactions within the lung and assessing potential antiviral treatments. Accordingly, the primary aim of this study is to develop and validate a Lung organoid-on-a-chip that transitions patient-derived 3D organoids into a 2D air-liquid interface culture within a microfluidic system. Through this approach, we demonstrate that the platform yields preliminary single-cell signatures concordant with conserved SARS-CoV-2 infection responses - consistent across four major variants - at single-cell resolution, providing mechanistic insights into viral pathogenesis and establishing a physiologically relevant platform for antiviral therapeutic evaluation.

Methods

Human lung organoid culture

Human distal airway organoids were established from patient-derived lung tissue as previously described [10]. Single-cell suspensions were embedded in Growth Factor Reduced Matrigel in

organoid growth medium supplemented with Wnt conditioned medium (WntCM). Organoids were passaged every 7–10 days through passage 3. Detailed reagent information is provided in the Online Supplement.

Lung organoid-on-a-chip and co-culture

The BE-Transflow microdevice (BEOnChip, Spain) was used for all chip-based experiments. The apical chamber was coated with 50% Matrigel and seeded with organoid-derived single cells at 1×10^5 cells per well. Human umbilical vein endothelial cells (HUVECs; Lonza) were seeded into the basal channel at 5×10^6 cells/mL. Full co-culture and ALI culture optimization details are provided in the Online Supplement.

SARS-CoV-2 reporter virus particle and live virus infection

SARS-CoV-2 reporter virus particles (RVPs) expressing green fluorescent protein (GFP), representing Wuhan-Hu-1, Delta (B.1.617.2), and Omicron BA.1 strains (Integral Molecular, Philadelphia, PA, USA), were applied to the apical chamber (50 μL per chip) for 3 days under biosafety level 2 (BSL-2) conditions. For live virus experiments, four SARS-CoV-2 variants - Wuhan (NCCP No. 43326), Delta B.1.617.2 (NCCP No. 43390), Omicron BA.1.1 (NCCP No. 43411), and Omicron XBB.1 (NCCP No. 43428) - were obtained from the National Culture Collection for Pathogens (Korea) and used at a multiplicity of infection of 0.2 under biosafety level 3 (BSL-3) conditions. Cells were harvested at 48 hours post-infection for downstream analyses. THP-1-derived macrophages were incorporated into the basal channel as described in the Online Supplement.

Single-cell RNA sequencing and bioinformatic analysis

Single-cell libraries were constructed using the Chromium Next GEM Single Cell 3’ Reagent Kit v3.1 (10x Genomics) and sequenced on an Illumina NovaSeq 6000 platform across five groups:

Control, Wuhan, Delta, Omicron BA.1, and Omicron XBB.1. Raw reads were processed with CellRanger (v7.0.1) against the GRCh38-2020-A reference. Cells with total unique molecular identifier (UMI) counts or detected gene counts below 5 median absolute deviations (MAD) from the median on a log-transformed scale were excluded. Additionally, cells exhibiting low transcriptomic complexity were filtered out if their percentage of counts in the top 20 genes exceeded the median+5 MAD. To eliminate potential apoptotic cells, those with a mitochondrial read ratio exceeding the lower threshold between the median + 3MAD or an absolute 12% limit were removed. Finally, doublets were identified and excluded using the Scrublet [11]. The remaining quality-filtered cells from each sample were integrated using scVI (v.1.4.0) [12] to perform batch correction across samples. Within the integrated data, log-normalization and unsupervised Leiden clustering at a resolution of 1.0 were executed. Subsequent cell-type annotation was performed using an internally established methodology based on canonical marker genes derived from literature (13-21), focusing on highly variable genes (HVGs). All downstream quantifications were performed using the log-normalized expression values, excluding cells labeled as unknown.

For downstream functional analysis, the gene set score was defined as the average expression of a target gene set minus the average expression of a randomly selected, expression-matched reference gene set [22]. Target pathways were sourced from the MSigDB Hallmark database, specifically including INTERFERON_ALPHA_RESPONSE, INTERFERON_GAMMA_RESPONSE, INFLAMMATORY_RESPONSE, TNFA_SIGNALING_VIA_NFKB, IL6_JAK_STAT3_SIGNALING, and APOPTOSIS. Additionally, literature-curated custom gene panels were utilized, comprising 11 epithelial markers (CDH1, EPCAM, CLDN3, CLDN4, CLDN7, OCLN, TJP1, KRT8, KRT18, KRT19,

and DSP), 7 mesenchymal markers (CDH2, VIM, FN1, S100A4, MMP2, MMP9, and ACTA2), and 6 VEGF-signaling genes (VEGFA, PGF, FLT1, KDR, NRP1, and NRP2; as shown in Figure 6E).

Results

1. Establishing Organoid Culture Conditions

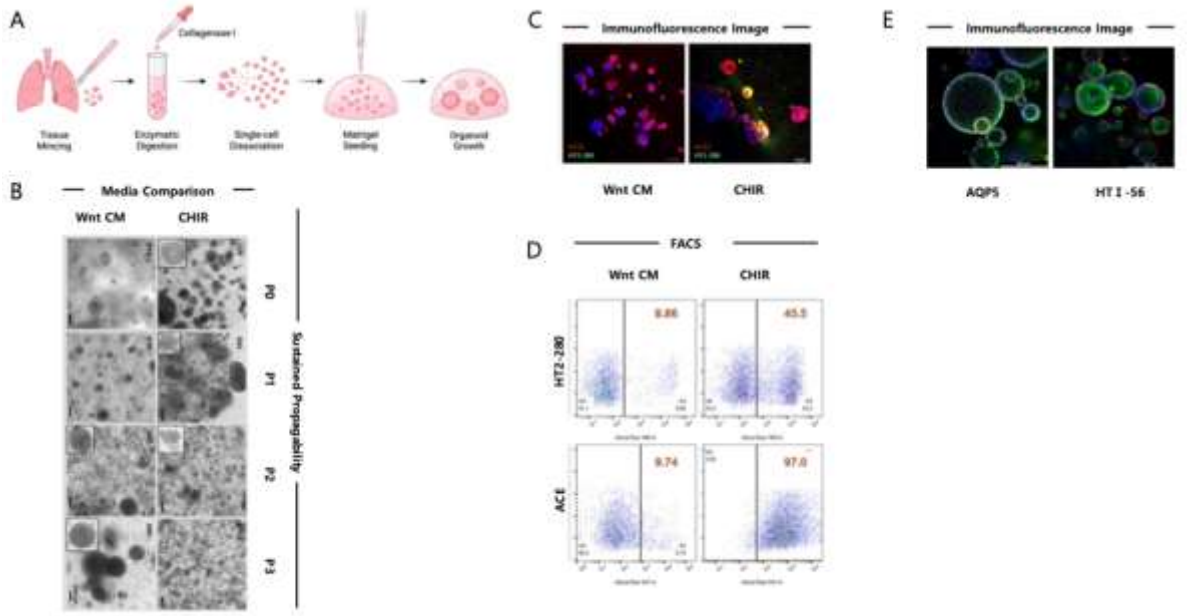


Figure 1. In Vivo-Like Lung Organoid model for Propagation and Differentiation

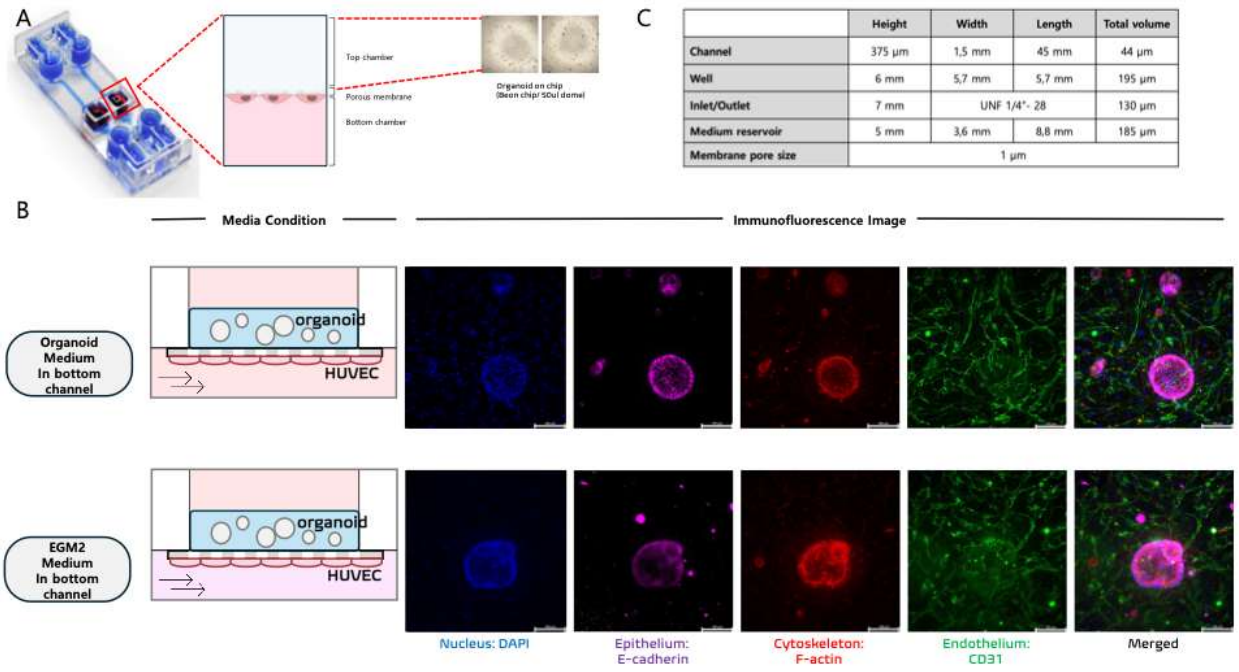
A. Schematic illustrating the main characteristics of lung tissue used as a source of adult stem cells for generating organoids. [Images created by Biorender]. B. Bright-field microscopy images of organoids cultured in 3D using different media. C. 3D organoids cultured in varied conditions were fixed, immunostained, and visualized using a Leica Thunder microscope. D. FACS analysis showing AT2 marker expression in organoids cultured under different media conditions. E. 3D organoids grown in WntCM media were fixed, immunostained, and visualized with Leica Thunder. These results suggest that WntCM was chosen as the optimal medium due to its capacity to support organoid differentiation, closely resembling the in vivo lung environment.

We compared two distinct media types, WntCM and CHIR, to evaluate their effects on organoid growth, stem cell maintenance, and differentiation. WntCM is known to activate the Wnt signaling pathway, essential in organoid culture for maintaining stemness and enabling self-

renewal. This pathway plays a key role in embryonic development, stem cell proliferation, and tissue regeneration by activating the Wnt/ β-catenin pathway [23]. In contrast, CHIR, a potent glycogen synthase kinase-3 (GSK-3) inhibitor, pharmacologically stimulates Wnt/β-catenin signaling, influencing cellular behavior differently. By inhibiting GSK-3, CHIR prevents the degradation of β-catenin, leading to its accumulation and the activation of Wnt target genes, rather than providing Wnt proteins directly [24,25]. This comparison allowed us to determine how each media condition impacts organoid development, particularly in terms of optimizing culture conditions for closely mimicking the *in vivo* lung environment or for our specific experimental need (i.e. SARS-CoV-2 infection). The adult lung organoid was cultured and passaged until passage 3 (P3), with its development regularly monitored using brightfield microscopy (Figure 1B). The growth and differentiation potential of lung organoids were evaluated by assessing the expression of two key lung-specific markers: HT2-280, associated with alveolar type II (AT2) cells, and angiotensin-converting enzyme 2 (ACE2), linked to epithelial function and known as the receptor for SARS-CoV-2. To compare two organoid media conditions, immunofluorescence (IF) staining confirmed the expression of HT2-280 and ACE2, and fluorescence-activated cell sorting (FACS) analysis was used to quantify the proportion of positive cells (Figure 1C, D). Notably, the proportion of HT2-280 and ACE2-expressing cells in the WntCM condition remained below 10%, closely resembling the percentage observed in *in vivo* lung tissue, indicating strong similarity in cellular composition [26]. The expression of aquaporin-5 (AQP-5) and HT1-56, key markers for alveolar type I (AT1) cells, was also confirmed in organoids cultured in WntCM (Figure 1E) [27]. Thus, WntCM was selected as the optimal culture condition for future experiments due to its ability to support organoid differentiation that closely mimics the *in vivo* lung environment.

Previously, in our lab, we conducted a single-cell RNA sequencing (scRNA-seq) analysis to investigate transcriptomic differences among four lung organoid culture in transwell models: O1 (3D organoid culture), O2 (organoid-derived 2D cells in WntCM media), EX (organoid-derived 2D cells in PneumaCult EX-plus media), and ALIEX (organoid-derived 2D cells under air-liquid interface conditions; ALIEX). Among these, the ALIEX model exhibited the highest transcriptomic similarity to *in vivo* lung epithelium, as demonstrated by comparison with Web-based Similarity Analysis System (W-SAS) lung tissue and Human Lung Cell Atlas (HLCA) normal lung parenchymal airway epithelial datasets. Single-cell RNA sequencing revealed that the ALIEX model had the highest proportion of ciliated cells (12.5%) while maintaining a significantly lower basal cell proportion, resembling the cellular composition of native airway epithelium. Furthermore, differential gene expression analysis identified key regulatory pathways associated with epithelial differentiation, including the downregulation of VEGFA and upregulation of CDKN1A, which were linked to enhanced ciliated cell differentiation. RNA velocity and pseudotime trajectory analysis further indicated a more advanced differentiation state in the ALIEX model, with a clear transition toward a ciliated cell fate, unlike other models that retained a higher proportion of undifferentiated basal cells. Based on these findings, we integrated an ALI culture system within a microfluidic Lung organoid-on-a-chip using the BEOnChip system. This platform was designed to support lung organoid-derived transitional differentiated cells under ALI conditions while simultaneously allowing co-culture with vascular endothelial cells. Given that the ALI model provided the most physiologically relevant epithelial differentiation profile, we prioritized incorporating ALI conditions in the Lung organoid-on-a-chip to optimize the epithelial-endothelial interface.

2. Establishing Co-culture Conditions for Organoid-Vascular Endothelial Cell Integration in a Lung organoid-on-a-chip



C

	Height	Width	Length	Total volume
Channel	375 μm	1,5 mm	45 mm	44 μm
Well	6 mm	5,7 mm	5,7 mm	195 μm
Inlet/Outlet	7 mm	UNF 1/4"- 28		130 μm
Medium reservoir	5 mm	3,6 mm	8,8 mm	185 μm
Membrane pore size	1 μm			

Figure 2. Culture of Lung organoid-on-a-chip

A. Schematic cross-sectional illustration of the top chamber and bottom channel. The dome-shaped organoids seeded on the chip were imaged using bright-field microscopy. B. 3D organoids co-cultured with HUVECs in the bottom channel were fixed, immunostained, and visualized using a Leica Thunder microscope. This schematic represents the co-culture system, where organoids are seeded in the top chamber, HUVECs are seeded in the bottom channel, and media tests were conducted. The findings suggest that WntCM was selected as the optimal medium, supporting organoid differentiation and closely mimicking the in vivo lung environment. C. The table presents the specifications of the BeonChip device. The device is made from cyclic olefin polymer (COP) and consists of two separate culture wells connected by a 1 μm porous polycarbonate membrane.

We utilized the BEOnChip platform to optimize the microfluidic model for a more realistic simulation of human physiological systems. This platform supports organoid culture, enables an ALI culture for epithelial cells with an open-top structure, and allows for the co-culture of lung organoids with vascular endothelial cells, enhancing the model's functionality (Figure 2A, C). In this study, we aimed to establish optimal conditions for co-culturing lung organoids with vascular endothelial cells in a BEOnChip system. After embedding the organoids in ECM, they

were seeded into the top chamber of the BEOnChip device and HUVECs were introduced into the bottom channel. To determine the optimal conditions for maintaining both organoid morphology and endothelial stability, two media conditions were tested in the bottom channel: organoid growth media (WntCM) and endothelial cell media (EGM™-2). The morphology and integrity of the co-cultured organoids were assessed using IF staining and visualized with the Leica Thunder imaging system (Figure 2B). The results showed that both organoid and endothelial media supported the stable maintenance of endothelial cells in the bottom channel. This was confirmed through CD31 immunostaining, which highlighted the formation of a microvascular network beneath the respiratory epithelium. However, the use of EGM™-2 media in the bottom channel resulted in a significant reduction of E-cadherin expression in the organoids, indicating a disruption in epithelial integrity. On the other hand, Organoids cultured in WntCM maintained stable E-cadherin and F-actin expression, indicating preserved epithelial integrity throughout the experiment (Figure 2B). This study demonstrated that organoid media is optimal for maintaining epithelial integrity in lung organoid-endothelial co-cultures, preserving E-cadherin expression, unlike endothelial media, which led to its reduction.

In a transwell system, HUVEC monoculture was also conducted to assess the stability of endothelial cells in various media conditions. We tested endothelial cell stability in organoid media (WntCM and CHIR) as well as a mixture of organoid media and EGM™-2. This experiment aimed to evaluate the impact of organoid media composition on endothelial cell stability for future co-culture in the Lung organoid-on-a-chip. Results indicated that endothelial cells were more stable in the WntCM condition for over a week compared to the CHIR condition provided in supplementary (Figure S1).

3. RVP infection test on Lung organoid-on-a-chip

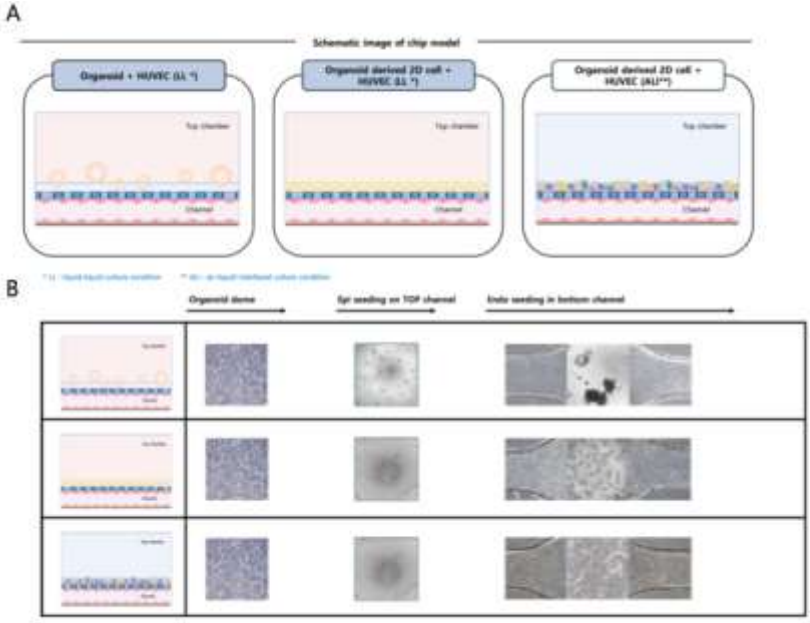


Figure 3. Culture of Lung organoid-on-a-chips and Air-liquid interface

A. Schematic representation showing three distinct experimental conditions tested in the Lung organoid-on-a-chip. We evaluated three setups where HUVECs were co-cultured in the bottom channel: [1] organoids cultured on Matrigel-coated chips, [2] organoid-derived 2D cells on chips, and [3] organoid-derived 2D cells differentiated under air-liquid interface (ALI) conditions.

B. Bright-field microscopy images displaying the organoid in the top chamber, HUVECs in the bottom channel, and the progression through the ALI process.

To determine the optimal conditions for infection, GFP fluorescence was detected at 3-, 4-, and 7-days post-infection, with the highest signal intensity observed at day 7. However, the difference between 3 and 7 days was minimal, indicating that a 3-day incubation period is sufficient for infection assays while minimizing experimental duration. The RVP input volume also significantly impacted infection efficiency, with 50 µL yielding the highest GFP signal in a dose-dependent manner. These findings align with previous protocol recommendations suggesting 3-day incubation and 50 µL RVP input as the optimal conditions for infection assays (Integral Molecular, 2022) [28] (Figure S2).

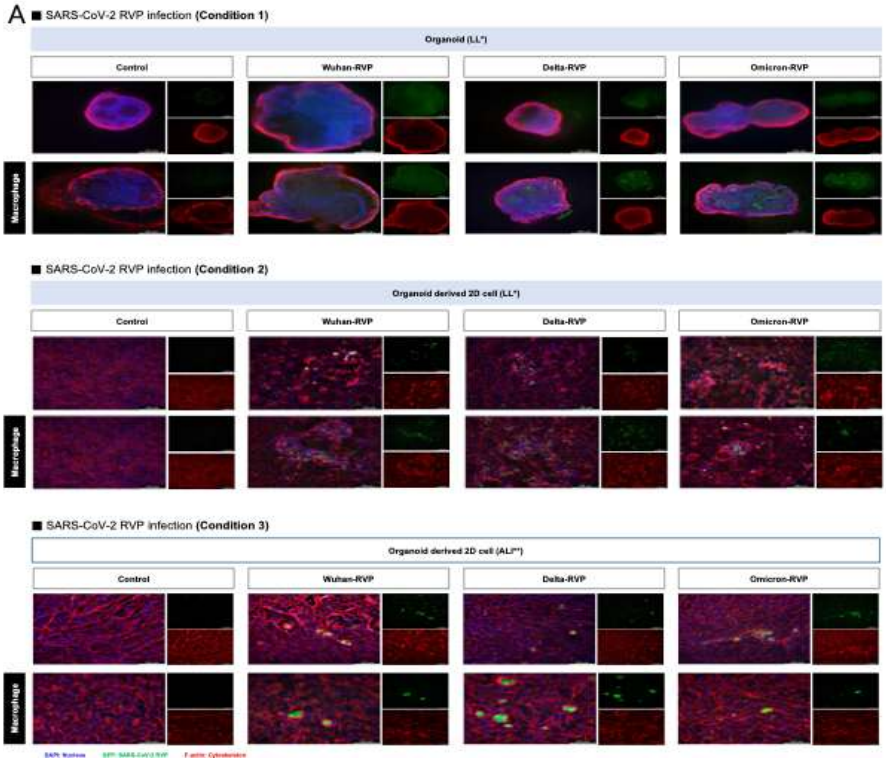


Figure 4. SARS-CoV-2 RVP infection test on Lung organoid-on-a-chip

A. IF staining images corresponding to experimental conditions (1–3) after infection with RVPs.

On a Lung organoid-on-a-chip, we tested three different conditions, where HUVECs were co-cultured in the bottom channel: [1] organoids cultured on Matrigel-coated chips, [2] organoid-derived 2D cells on chips, and [3] organoid-derived 2D cells differentiated in an ALI (Figure 3A, B). To enhance infection efficiency, organoids were converted to a 2D cell layer, and ALI differentiation was applied. Additionally, macrophages were introduced into the bottom channel with endothelial cells to further enhance infection efficiency. Each condition was infected with SARS-CoV-2 RVP-GFP strains (Wuhan, Delta, and Omicron) at 50 µL per chip for 3 days without media change to allow infection to progress.

As a result, no significant differences in infection rates were observed between viral strains, as

determined by fluorescence imaging. However, a notable increase in infection was observed in the presence of macrophages, suggesting that immune cell interactions may enhance viral entry or replication (Figure 4, Figure S3). These findings provide insights into infection dynamics and serve as a foundation for future studies using live SARS-CoV-2.

4. Single-cell transcriptomic profiling and cell-type identification in the Lung organoid-on-a-chip

To characterize cell-type-specific transcriptional responses to SARS-CoV-2 infection within the Lung organoid-on-a-chip, we performed scRNA-seq across five samples: Control, Wuhan, Delta, Omicron BA.1 (Omicron 1), and Omicron XBB.1 (Omicron 2). The global landscape of the integrated dataset indicates well-mixed distribution of cells across the control and 4 different strains without strong batch effects (Figure 5A).

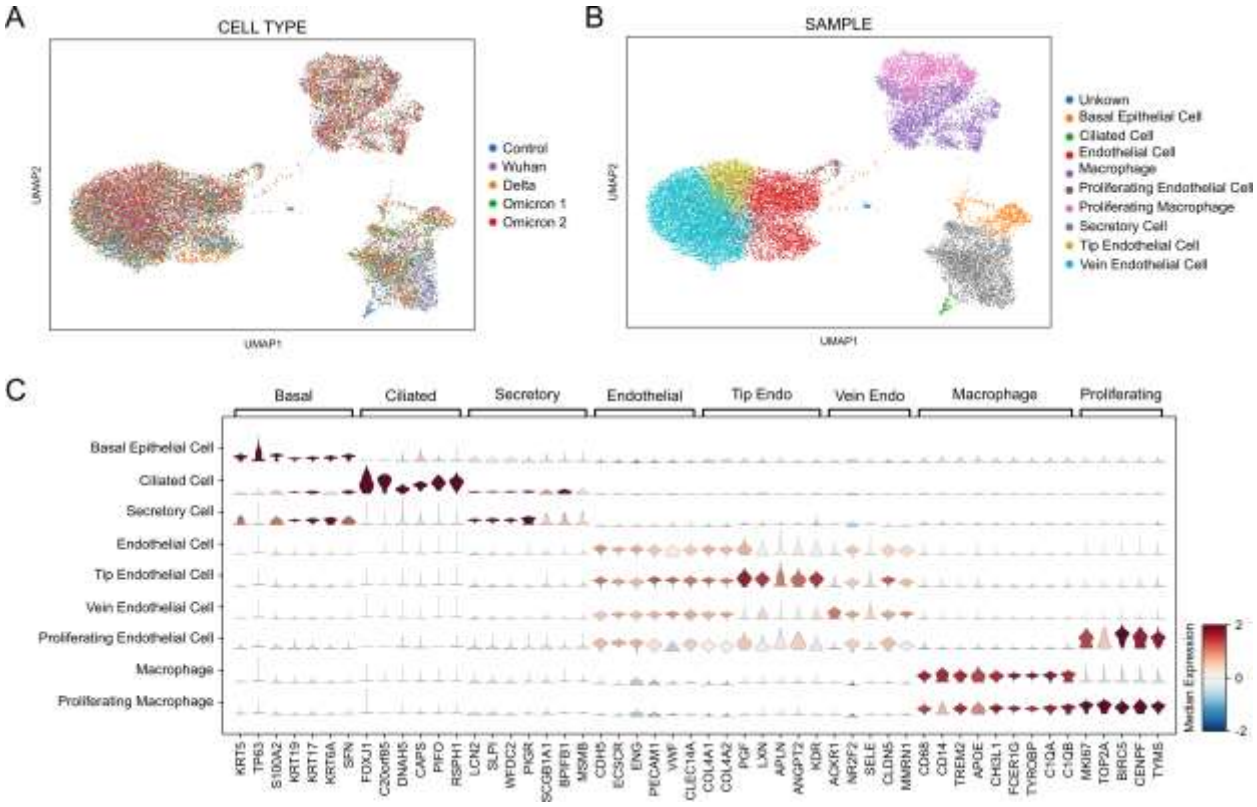
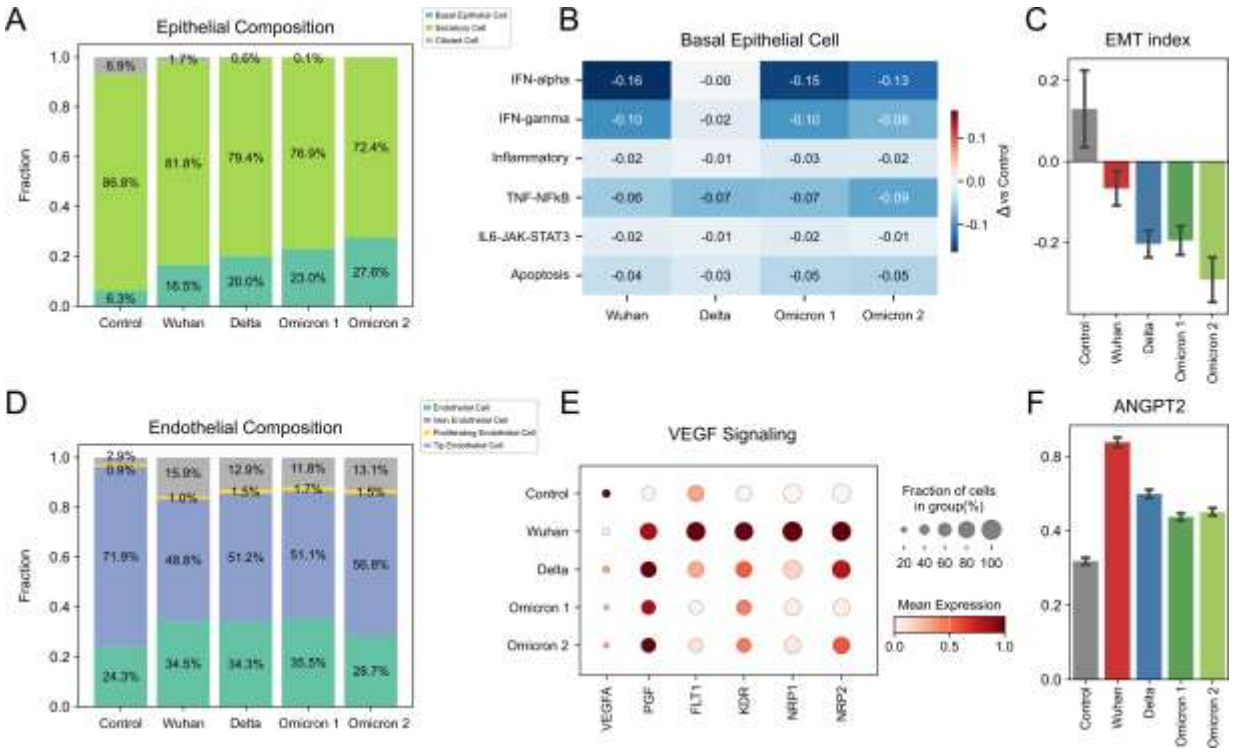


Figure 5. Cell-type annotation of the Lung organoid-on-a-chip scRNA-seq dataset.

(A) Uniform Manifold Approximation and Projection (UMAP) embedding of the integrated Lung organoid-on-a-chip scRNA-seq dataset colored by sample (Control, Wuhan, Delta, Omicron 1, and Omicron 2). (B) UMAP feature plots showing 10 distinct cell types. (C) Stacked violin plot of canonical marker genes across the cell types.

Based on Leiden clustering, we classified the integrated dataset into 10 distinct cell types (Figure 5B). These cell types were broadly classified into three major lineages: epithelial, endothelial, and immune compartments. Specifically, the epithelial lineage comprised ciliated cells, club cells, basal epithelial cells. The endothelial compartment included general endothelial cells, vein endothelial cells, and proliferating endothelial cells, while the immune compartment was represented by macrophages and proliferating macrophages. The distinct transcriptomic identities of these assigned populations were clearly demonstrated by their cell-type-specific marker expression profiles (Figure 5C).



294 **Figure 6. Changes in epithelial and endothelial cells in the Lung organoid-on-a-chip.**

295 **(A) Stacked bar plots illustrate the proportional changes of epithelial sub-populations across the control and four strains. (B) Heatmap of**

296 **host-response gene-set scores (IFN-α/γ, inflammatory, TNF-NFκB, IL-6/JAK/STAT3, apoptosis) shown as the change relative to control**

297 **in basal epithelial cells. (C) Bar plots of the mean EMT index, defined as the difference between epithelial and mesenchymal marker**

298 **gene-set scores, in basal epithelial cells across the control and four strains. (D) Stacked bar plots illustrate the proportional changes of**

299 **endothelial sub-populations across the control and four strains. (E) Standardized expression of VEGF signaling pathway-related genes**

300 **within the endothelial cells across the control and four strains. (F) Mean ANGPT2 expression within the general endothelial + vein**

301 **endothelial subset across the control and four strains.**

302

303 To evaluate infection-associated cellular dynamics, we compared the relative proportions of

304 epithelial subtypes across samples (Figure 6A). Notably, a marked reduction in the proportion of

305 ciliated cells was observed, decreasing from 6.9% in the control to a minimum of 0.0% in the

306 infected group. Conversely, basal cells expanded progressively, rising from 6.3% in the control

307 to a maximum of 27.6% under Omicron.

308 To assess the host transcriptional response in basal epithelial cells, we scored host-defense

309 related gene-set scores (IFN-α, IFN-γ, inflammatory, TNF-NFκB, IL-6/JAK/STAT3, and

apoptosis) and compared each variant to the control (Figure 6B). All pathways were reduced relative to control across four strains. The reduction was most pronounced for the interferon pathways, with the IFN-α related gene expression decreasing by up to 0.16.

We also examined the epithelial-mesenchymal balance in basal cells using an EMT index (epithelial - mesenchymal marker module scores; positive = epithelial dominant, Figure 6C). The index was positive only in the control (+0.13) and turned negative in all four variants (-0.07 to -0.29), showing a consistent shift away from the epithelial state upon infection. Within the endothelial compartment, the tip (angiogenic) endothelial fraction rose from 2.9% in the control to maximum 15.7% in the infected samples (Figure 6D). Consistent with this angiogenic shift, VEGF-signaling genes were broadly upregulated in endothelial cells, including PGF, KDR, and the co-receptors NRP1/NRP2, whereas the ligand VEGFA was the only member to decrease. ANGPT2 expression in the combined general and vein endothelial subset was higher in all four strains than in the control (Figure 6F).

Discussion

The primary achievement of this study lies in the successful establishment of an advanced Lung organoid-on-a-chip platform, derived from patient-derived distal airway organoids, capable of stably modeling infections from a broad range of SARS-CoV-2 variants. By integrating a 3D organoid-derived 2D ALI epithelial layer with vascular endothelial cells and immune components within a microfluidic device, we demonstrated that four major variants - Wuhan, Delta, Omicron BA.1, and Omicron XBB.1 - can effectively infect this integrated system. These findings underscore that the study's main point is the development of a versatile infectious disease research platform capable of reproducing human-relevant infection responses regardless of the specific viral variant. The integration of an ALI culture system within the BEOnChip microfluidic platform was informed by prior transcriptomic evidence from our group demonstrating that the ALI-differentiated model most closely recapitulates the cellular composition of native airway epithelium, with enriched multiciliated cell fractions and a reduced basal cell proportion [10]. This pattern is consistent with physiological mucociliary differentiation driven by Notch-FOXJ1 signaling [29, 30]. The selection of WntCM as the unified culture medium across both compartments further ensured epithelial integrity throughout this transition, as WntCM preserved E-cadherin and F-actin organization in the epithelial layer - unlike EGM-2, whose constituent growth factors are known to downregulate E-cadherin via extracellular signal-regulated kinase/mitogen-activated protein kinase (ERK/MAPK) signaling [31, 32] - while maintaining stable endothelial morphology confirmed by CD31 staining, addressing a common challenge of medium-mediated cross-compartment interference in organ-on-chip co-culture systems [33].

Prior to live virus experiments, SARS-CoV-2 RVP infection assays were conducted across three

platform configurations to confirm viral entry competency under BSL-2 conditions. The absence of significant inter-variant differences in GFP fluorescence was anticipated, as replication-incompetent RVPs are inherently limited to a single round of ACE2-mediated entry and cannot resolve the strain-specific differences in replication kinetics or immune evasion that emerge with live virus [34]. These results nonetheless validated the platform's susceptibility to SARS-CoV-2 entry across all tested conditions, providing the necessary foundation for subsequent live virus experiments in which variant-specific transcriptomic responses were characterized at single-cell resolution. In this study, we validated the suitability of our Lung organoid-on-a-chip for virus research. To observe whether the model behaves similar to the lung *in vivo*, we tested 4 different COVID-19 strains and compared the responses of the Lung organoid-on-a-chip against control. One of the major observations in our dataset is a marked reduction in ciliated cells, accompanied by a relative increase in the proportion of basal epithelial cells. This is consistent with the basal stem cell–driven regeneration that follows airway epithelial injury after SARS-CoV-2 infection [35]. The uniform reduction of host-defense gene-set scores in infected basal cells, most pronounced for the interferon pathways, is in line with the characteristically blunted type I/III interferon response that defines SARS-CoV-2 infection of the respiratory epithelium [36, 37], and the broad downregulation across modules is consistent with nonstructural protein (NSP) 1-mediated host shutoff [38, 39]. The EMT index turned negative across all infected samples, indicating a shift away from epithelial identity in basal cells. This reflected a coordinated change - a loss of epithelial markers together with a gain of mesenchymal markers - that was consistent across all four variants. Such an EMT-like, profibrotic priming of the airway epithelium has been described in COVID-19 lung [40, 41]. In the endothelium, the tip (angiogenic) endothelial cell fraction expanded, and VEGF-signaling genes were broadly upregulated, suggesting angiogenic

reprogramming. Notably, the VEGFA-low, ANGPT2-high angiogenic signature is compatible with VEGF-independent angiogenesis, a mode that includes the intussusceptive angiogenesis reported in COVID-19 lungs [42, 43]. ANGPT2 is, moreover, a well-recognized marker of endothelial activation and vascular leak in SARS-CoV-2 infection [44, 45].

This study has several limitations. First, with only one sample per condition, statistical validation was not feasible. The transcriptomic changes reported here should be regarded as preliminary observations awaiting confirmation by biological replication. We note, however, that each reported directional change - ciliated-cell loss with basal expansion, blunted interferon scores, EMT-like priming, angiogenic tip-cell expansion, and ANGPT2 induction - independently matches the direction of previously published in vivo and patient-derived COVID-19 signatures cited above [35-45]. It is unlikely that a technical artifact arising from a single chip would simultaneously and consistently reproduce the directional patterns of multiple previously reported biological signatures. Accordingly, the high degree of concordance with prior studies provides meaningful support for interpreting the observed transcriptomic responses as infection-driven biological changes rather than as consequences of batch effects. Second, gene-set scores reflect transcriptional (mRNA) changes and thus have limited power to capture protein- or function-level events such as vascular leak; for host shutoff in particular, a decreased score cannot distinguish immune evasion from reduced viral replication. Third, to first establish and validate the integrated multi-compartment platform in a robust manner, the vascular and immune channels were reconstituted with well-characterized, and highly reproducible cell sources - human umbilical vein endothelial cells (HUVECs) and THP-1 derived macrophages - with which the key endothelial responses to SARS-CoV-2 infection were successfully recapitulated. However, because HUVECs are of venous origin, these responses are more appropriately

interpreted as those of an activated endothelium rather than as lung-microvascular–specific responses.

In future studies, these compartments will be enhanced by integrating lung microvascular endothelial cells and macrophage sources better suited to the pulmonary environment, thereby more closely recapitulating the native lung microenvironment. In parallel, the findings will be validated through adequately powered biological replication across multiple SARS-CoV-2 variants.

Conclusion

In summary, this study successfully transitioned patient-derived lung organoids into a 2D ALI culture within a Lung organoid-on-a-chip, establishing a viral infection model that accurately recapitulates the human lung microenvironment. Notably, using scRNA-seq, we demonstrated the platform's robust analytical capability by capturing high-resolution pathological signatures across four major SARS-CoV-2 variants - including a loss of ciliated cells with a relative increase in basal cells, a broad suppression of the epithelial host-defense program shutoff, an EMT-like priming of basal epithelial cells, and an angiogenic reprogramming of the endothelial cells marked by ANGPT2 induction. Despite limitations regarding biological replicates, this platform proves its potential as an ethical and efficient tool for drug screening and viral pathophysiology research by precisely simulating in vivo responses, offering a viable alternative to animal models. Moving forward, this model is expected to serve as a versatile rapid-response platform for future pandemics and a cornerstone technology for the advancement of personalized precision medicine.

List of abbreviations

ALI	Air Liquid Interface
EMT	Endothelial Mesenchymal Transition
HUVEC	Human Umbilical Vein Endothelial Cell
HVG	Highly Variable Gene
HLCA	Human Lung Cell Atlas

Declarations

Ethical approval and consent to participate

Human lung tissue samples were collected with written informed consent and ethical approval from the Institutional Review Board of Seoul National University Bundang Hospital. All procedures were conducted in accordance with the principles of the Declaration of Helsinki.

Consent for publication

Not applicable

Availability of data and materials

The single-cell RNA sequencing data generated in this study will be deposited in a public repository (e.g., Gene Expression Omnibus) upon acceptance. All other data are available from the corresponding authors upon reasonable request.

Competing Interests

The authors declare that they have no competing interests.

Funding

This research was supported by the Seoul National University Bundang Hospital Research Fund (grant number 18-2023-0008) to Y.J.C. This work was supported by the National Research Foundation of Korea (NRF) grant funded by the Korea government (MSIT) (No. RS-2023-00278658), Bio&Medical Technology Development Program of the National Research Foundation (NRF) funded by the Korean government (MSIT) (No. RS-2024-00439078), and HRD Program for Industrial Innovation through the Korea Institute for Advancement Technology (KIAT) funded by the Ministry of Trade, Industry and Energy (RS-2025-02214034) to J.P.

Authors' Contributions

S.P. and S.H.K. contributed equally to this work. S.P., B.K., and E.Y.E. performed the experiments. S.H.K. performed single-cell RNA sequencing analysis and data curation. Y.J. contributed to the single-cell RNA sequencing analysis. H.J.K. provided supervision and critical review. J.P. and Y.J.C. conceived and supervised the study and obtained funding. All authors reviewed and approved the final manuscript.

Acknowledgements

Not applicable

References

1. GBD 2019 Chronic Respiratory Diseases Collaborators. Global burden of chronic respiratory diseases and risk factors, 1990-2019: an update from the Global Burden of Disease Study 2019. eClinicalMedicine. 2023;59:101936. doi:10.1016/j.eclinm.2023.101936.
2. Rabbani G, Islam SMS, Rahman MA, Amin N, Marzan B, Robin RC, et al. Pre-existing COPD is associated with an increased risk of mortality and severity in COVID-19: a rapid systematic review and meta-analysis. Expert Rev Respir Med. 2021;15:705-16. doi:10.1080/17476348.2021.1866547.
3. Yang SH, Park EJ, Kim JH, Song JW, Cho YJ. Understanding of patients with severe COVID-19 using lung ultrasound. Tuberc Respir Dis (Seoul). 2025;88:380-7. doi:10.4046/trd.2024.0025.
4. Zhu L, Zhang J, Guo Q, Kuang J, Li D, Wu M, et al. Advanced lung organoids and lung-on-a-chip for cancer research and drug evaluation: a review. Front Bioeng Biotechnol. 2023;11:1299033. doi:10.3389/fbioe.2023.1299033.
5. Gkatzis K, Taghizadeh S, Huh D, Stainier DYR, Bellusci S. Use of three-dimensional organoids and lung-on-a-chip methods to study lung development, regeneration and disease. Eur Respir J. 2018;52:1800876. doi:10.1183/13993003.00876-2018.
6. Lancaster MA, Knoblich JA. Organogenesis in a dish: modeling development and disease using organoid technologies. Science. 2014;345:1247125. doi:10.1126/science.1247125.
7. Clevers H. Modeling development and disease with organoids. Cell. 2016;165:1586-97. doi:10.1016/j.cell.2016.05.082.
8. Fulcher ML, Gabriel S, Burns KA, Yankaskas JR, Randell SH. Well-differentiated human airway epithelial cell cultures. Methods Mol Med. 2005;107:183-206. doi:10.1385/1-59259-861-7:183.

9. Huh D, Matthews BD, Mammoto A, Montoya-Zavala M, Hsin HY, Ingber DE. Reconstituting organ-level lung functions on a chip. Science. 2010;328:1662-8. doi:10.1126/science.1188302.
10. Kim J, Eo EY, Kim B, Lee H, Kim J, Koo BK, et al. Transcriptomic analysis of air-liquid interface culture in human lung organoids reveals regulators of epithelial differentiation. Cells. 2024;13:1991. doi:10.3390/cells13231991.
11. Wolock SL, Lopez R, Klein AM. Scrublet: computational identification of cell doublets in single-cell transcriptomic data. Cell Syst. 2019;8:281-291.e9. doi:10.1016/j.cels.2018.11.005.
12. Lopez R, Regier J, Cole MB, Jordan MI, Yosef N. Deep generative modeling for single-cell transcriptomics. Nat Methods. 2018;15:1053-8. doi:10.1038/s41592-018-0229-2.
13. Deprez M, Zaragosi LE, Truchi M, Becavin C, Ruiz García S, Arguel MJ, et al. A single-cell atlas of the human healthy airways. Am J Respir Crit Care Med. 2020;202:1636-45. doi:10.1164/rccm.201911-2199OC.
14. Travaglini KJ, Nabhan AN, Penland L, Sinha R, Gillich A, Sit RV, et al. A molecular cell atlas of the human lung from single-cell RNA sequencing. Nature. 2020;587:619-25. doi:10.1038/s41586-020-2922-4.
15. Sikkema L, Ramírez-Suástegui C, Strobl DC, Gillett TE, Zappia L, Madissoon E, et al. An integrated cell atlas of the lung in health and disease. Nat Med. 2023;29:1563-77. doi:10.1038/s41591-023-02327-2.
16. Montoro DT, Haber AL, Biton M, Vinarsky V, Lin B, Birket SE, et al. A revised airway epithelial hierarchy includes CFTR-expressing ionocytes. Nature. 2018;560:319-24. doi:10.1038/s41586-018-0393-7.
17. Schupp JC, Adams TS, Cosme C, Raredon MSB, Yuan Y, Omote N, et al. Integrated single-

cell atlas of endothelial cells of the human lung. Circulation. 2021;144:286-302. doi:10.1161/CIRCULATIONAHA.120.052318.

18. Godoy RS, Cober ND, Cook DP, McCourt E, Deng Y, Wang L, et al. Single-cell transcriptomic atlas of lung microvascular regeneration after targeted endothelial cell ablation. Elife. 2023;12:e80900. doi:10.7554/eLife.80900.

19. Rohlenova K, Goveia J, García-Caballero M, Subramanian A, Kalucka J, Treps L, et al. Single-cell RNA sequencing maps endothelial metabolic plasticity in pathological angiogenesis. Cell Metab. 2020;31:862-877.e14. doi:10.1016/j.cmet.2020.03.009.

20. Zilionis R, Engblom C, Pfirschke C, Savova V, Zemmour D, Saatcioglu HD, et al. Single-cell transcriptomics of human and mouse lung cancers reveals conserved myeloid populations across individuals and species. Immunity. 2019;50:1317-1334.e10. doi:10.1016/j.immuni.2019.03.009.

21. Mould KJ, Moore CM, McManus SA, McCubbrey AL, McClendon JD, Griesmer CL, et al. Airspace macrophages and monocytes exist in transcriptionally distinct subsets in healthy adults. Am J Respir Crit Care Med. 2021;203:946-56. doi:10.1164/rccm.202005-1989OC.

22. Tirosh I, Izar B, Prakadan SM, Wadsworth MH, Treacy D, Trombetta JJ, et al. Dissecting the multicellular ecosystem of metastatic melanoma by single-cell RNA-seq. Science. 2016;352:189-96. doi:10.1126/science.aad0501.

23. Nusse R, Clevers H. Wnt/beta-catenin signaling, disease, and emerging therapeutic modalities. Cell. 2017;169:985-99. doi:10.1016/j.cell.2017.05.016.

24. Bain J, McLauchlan H, Elliott M, Cohen P. The specificities of protein kinase inhibitors: an update. Biochem J. 2003;371:199-204. doi:10.1042/BJ20021535.

25. Ying QL, Wray J, Nichols J, Batlle-Morera L, Doble B, Woodgett J, et al. The ground state

of embryonic stem cell self-renewal. Nature. 2008;453:519-23. doi:10.1038/nature06968.

26. Crapo JD, Barry BE, Gehr P, Bachofen M, Weibel ER. Cell number and cell characteristics of the normal human lung. Am Rev Respir Dis. 1982;126:332-7. doi:10.1164/arrd.1982.126.2.332.

27. Dobbs LG, Gonzalez RF, Allen L, Froh DK. HTI56, an integral membrane protein specific to human alveolar type I cells. J Histochem Cytochem. 1999;47:129-37. doi:10.1177/002215549904700202.

28. Integral Molecular. Infectivity of SARS-CoV-2 GFP reporter virus particles (RVPs), version 6. https://www.integralmolecular.com/sarscov2rvpdocuments/. Accessed 27 Jul 2026.

29. Rock JR, Onaitis MW, Rawlins EL, Lu Y, Clark CP, Xue Y, et al. Basal cells as stem cells of the mouse trachea and human airway epithelium. Proc Natl Acad Sci U S A. 2009;106:12771-5. doi:10.1073/pnas.0906850106.

30. Tsao PN, Vasconcelos M, Izvolsky KI, Qian J, Lu J, Bhatt DL, et al. Notch signaling controls the balance of ciliated and secretory cell fates in developing airways. Development. 2009;136:2297-307. doi:10.1242/dev.034884.

31. Lo HW, Hsu SC, Xia W, Hua X, Lam YC, Hafner M, et al. Epidermal growth factor receptor cooperates with STAT3 to induce epithelial-mesenchymal transition in cancer cells via up-regulation of TWIST gene expression. Cancer Res. 2007;67:9066-76. doi:10.1158/0008-5472.CAN-07-0575.

32. Yang J, Antin P, Berx G, Bhatt D, Bhatt DL, Brabletz T, et al. Guidelines and definitions for research on epithelial-mesenchymal transition. Nat Rev Mol Cell Biol. 2020;21:341-52. doi:10.1038/s41580-020-0237-9.

33. Ingber DE. Human organs-on-chips for disease modelling, drug development and

personalized medicine. Nat Rev Genet. 2022;23:467-91. doi:10.1038/s41576-022-00466-9.

34. Schmidt F, Weisblum Y, Muecksch F, Hoffmann HH, Gaebler C, Lorenzi JCC, et al. Measuring SARS-CoV-2 neutralizing antibody activity using pseudotyped and chimeric viruses. J Exp Med. 2020;217:e20201181. doi:10.1084/jem.20201181.

35. Chen M, Pekosz A, Villano JS, Shen W, Zhou R, Kulaga H, et al. Evolution of nasal and olfactory infection characteristics of SARS-CoV-2 variants. J Clin Invest. 2024;134:e174439. doi:10.1172/JCI174439.

36. Blanco-Melo D, Nilsson-Payant BE, Liu WC, Uhl S, Hoagland D, Møller R, et al. Imbalanced host response to SARS-CoV-2 drives development of COVID-19. Cell. 2020;181:1036-1045.e9. doi:10.1016/j.cell.2020.04.026.

37. Alfi O, Yakirevitch A, Wald O, Wandel O, Izhar U, Oiknine-Djian E, et al. Human nasal and lung tissues infected ex vivo with SARS-CoV-2 provide insights into differential tissue-specific and virus-specific innate immune responses in the upper and lower respiratory tract. J Virol. 2021;95:e0013021. doi:10.1128/JVI.00130-21.

38. Thoms M, Buschauer R, Ameismeier M, Koepke L, Denk T, Hirschenberger M, et al. Structural basis for translational shutdown and immune evasion by the Nsp1 protein of SARS-CoV-2. Science. 2020;369:1249-55. doi:10.1126/science.abc8665.

39. Fisher T, Gluck A, Narayanan K, Kuroda M, Nachshon A, Hsu JC, et al. Parsing the role of NSP1 in SARS-CoV-2 infection. Cell Rep. 2022;39:110954. doi:10.1016/j.celrep.2022.110954.

40. Zhang L, Tang C, Zhang M, Tong X, Xie Y, Yan R, et al. Single cell meta-analysis of EndMT and EMT state in COVID-19. Front Immunol. 2022;13:976512. doi:10.3389/fimmu.2022.976512.

41. Niayesh-Mehr R, Kalantar M, Bontempi G, Montaldo C, Ebrahimi S, Allameh A, et al. The role of epithelial-mesenchymal transition in pulmonary fibrosis: lessons from idiopathic pulmonary fibrosis and COVID-19. Cell Commun Signal. 2024;22:542. doi:10.1186/s12964-024-01925-y.
42. Abdullah SE, Perez-Soler R. Mechanisms of resistance to vascular endothelial growth factor blockade. Cancer. 2011;118:3455-67. doi:10.1002/cncr.26540.
43. Jonigk D, Werlein C, Lee PD, Kauczor HU, Länger F, Ackermann M. Pulmonary and systemic pathology in COVID-19-holistic pathological analyses. Dtsch Arztebl Int. 2022;119:429-35. doi:10.3238/arztebl.m2022.0231.
44. Spadaro S, Fogagnolo A, Campo G, Zucchetti O, Verri M, Ottaviani I, et al. Markers of endothelial and epithelial pulmonary injury in mechanically ventilated COVID-19 ICU patients. Crit Care. 2021;25:74. doi:10.1186/s13054-021-03499-4.
45. Price DR, Benedetti E, Hoffman KL, Gomez-Escobar L, Alvarez-Mulett S, Capili A, et al. Angiopoietin 2 is associated with vascular necroptosis induction in coronavirus disease 2019 acute respiratory distress syndrome. Am J Pathol. 2022;192:1001-15. doi:10.1016/j.ajpath.2022.04.002.

Supplementary Files

This is a list of supplementary files associated with this preprint. Click to download.

- SupplementaryMaterials.docx